IEEE Access
Multidisciplinary | Rapid Review | Open Access Journal

Received March 26, 2021, accepted May 17, 2021, date of publication May 31, 2021, date of current version June 9, 2021.

Digital Object Identifier 10.1109/ACCESS.2021.3085029

A Common DC-Bus-Configured Traction Motor Emulator Using a Virtually Isolated Three-Phase AC-DC Bidirectional Converter

ARVIND H. KADAM, (Member, IEEE), AND SHELDON S. WILLIAMSON, (Fellow, IEEE)
Smart Transportation Electrification and Energy Research (STEER) Group, Department of Electrical, Computer and Software Engineering, Faculty of Engineering and Applied Sciences (FEAS), Ontario Tech University (University of Ontario Institute of Technology), Oshawa, ON L1G 0C5, Canada

Corresponding author: Arvind H. Kadam (arvind.h.kadam@ieee.org)

ABSTRACT An industrial drive testing, with a 'real-machine' can pave way, for some serious issues to test-bench and motor. A slight disturbance in control logic amid testing, can damage the physical machine or drive. Such dangerous testing conditions can be avoided by supplanting real motor with a power electronic converter based 'Motor Emulator' (ME) test-bench system. The conventional ME comprises of two-stage three-phase AC-DC-AC conversion with first-stage AC-DC as emulator and second-stage DC-AC as regenerating unit. This two-stage power conversion, require independent control algorithm, burdening control complexity as well as the number of power electronic switches are quite significant. Hence, to economize and downsize conventional multistage ME system, this paper experimentally validates a common DC-bus-configured ME system with only the AC-DC regenerative emulator stage. A virtually isolated bidirectional two-level three-phase AC-DC converter is proposed as the regenerative emulator converter in a common DC-Bus-configured ME system. The Proposed converter's operating principle along with mathematical design and control strategy are also presented. To validate the operation of the proposed converter as a common DC-bus-configured emulator, a permanent magnet synchronous motors (PMSM) of *7.5 kW* is emulated and its experimental results are presented here.

INDEX TERMS AC-DC, bidirectional converter, buck-boost, DC-AC, device under test, motor emulator, permanent magnet synchronous motor, synchronous converter, virtual isolation.

I. INTRODUCTION

Testing of commercial product for quality control is of prime importance in any production industry. In the electric drive manufacturing industry, the drive should be tested in the production stage for its control, robustness, power level, protection as well as fault detection capabilities. The conventional test-rig setup with the real electric machine for testing the motor drives has some drawbacks, such as extended test time, huge space requirement, high energy consumption, higher operation and maintenance cost as well as large equipment complexity. The need of replacing physical electric motor for testing drive at various load configuration, further adds on operating cost and complexity of the system.

Integration of power electronics together with software simulation is being used for developing a hardware-in-loop (HIL) system for emulating an electric motor [1]. This power electronic system capable of emulating motor characteristics is known as 'motor emulator' (ME). In traditional ME, real rotating machine is replaced with AC-DC-AC multistage, power electronic converter [2], [3]. The motor model estimates the phase, frequency and magnitude of current for a specific motor for the applied voltage input at motor terminals by drive [4]. Further, based on control strategy implemented, the emulating converter is controlled in such a way that, current drawn from 'Device Under Test' *or* 'Drive Under Test' (DUT) mimics the estimated reference current by motor model. The advantage of such ME system is, flexible load configuration. By changing parameters in motor model and control loop, ME starts emulating an all new motor [3], eliminating need for replacing real physical motor as well as restructuring of the test-bench setup.

A. CONCEPT OF MOTOR EMULATOR

According to [4], the primary goal of traction motor emulator is to design and develop a power electronics converter based

The associate editor coordinating the review of this manuscript and approving it for publication was Tariq Masood.

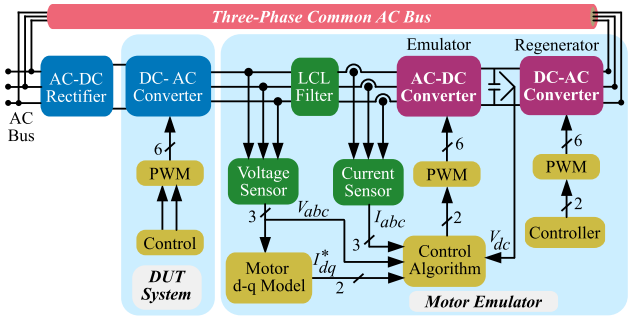

FIGURE 1. Block diagram of classical motor emulator.

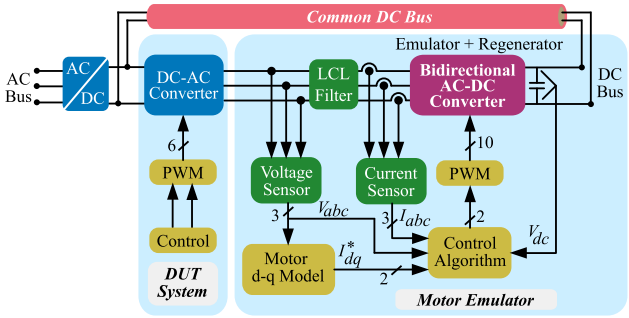

FIGURE 2. Block diagram of common DC-bus-configured motor emulator.

controlled load as an replacement for the actual traction machine load. Subsequently, the behavior of the traction machine emulator should be as close as the electrical characteristics of the real traction machine load when driven by a DUT.

The traditional traction motor emulator configuration is as demonstrated in Fig. 1, where the emulator converter is driven by the three-phase DUT output voltage. Thus, detailed information of the phase, frequency and magnitude of the DUT output voltages is of prime importance.

The core element of traction motor emulator is the mathematical model of electric motor under emulation, that estimates the phase frequency and magnitude of the desired currents to be drawn so as to imitate the real electric machine. Further, the control algorithm ensures that three-phase currents drawn or supplied by the ME are matching with that of the estimated current references.

The ME is driven by the DUT and both the power electronics converters coupled to each other through L or LCL filter. Since the ME imitates the electrical characteristics of an real electric traction motor, it would have to either absorb or supply power as per the quadrant of operation of the electric motor under emulation. To empower the ME to be a '*sink*' or '*source*' of power, two back-to-back VSI (voltage source inverter) forming a two-level AC-AC cyclo-converter is used. The dc link element is common to both emulator and re-generator VSI. The three-phase voltage output of re-generator VSI converter is fed to the AC utility grid. This re-generator VSI absorbs or supplies power from the utility grid for the emulator VSI.

B. STRUCTURE OF MOTOR EMULATOR

A ME system comprises of two back-to-back AC-DC and DC-AC power converters as shown in Fig. 1. Where former, operates as an *emulator* and later as a *regenerating unit* [1]–[6]. The output of regeneration unit is interfaced with utility grid, to act as 'sink' or 'source' in case of motoring or regenerative braking operation respectively. This two-stage arrangement forming AC-AC PWM (*pulse width modulation*) Cycloconverter with common DC link capacitor, requires independent control and increases controller complexity [4]. The dc-link element ensures the decoupling between two converter stages [7]. This entrench that, a constant source is available at the input of DC-AC inverter stage, which increases the converter's power capability. However, the dc-link element can have a relatively large size compared with the total converter size [7].

To simplify the control algorithm and to reduce the number of converter stages, a common DC-bus ME system architecture was presented by [8], where output of the AC-DC converter stage is fed back to DC source of the DUT. The structure of ME with common DC bus is shown in Fig. 2, where DUT input as well as DC side of the proposed converter are supplied with a common DC source. Unlike the system shown in Fig. 1, where three-phase AC output of the regenerator converter is fed back to the utility, the output power of proposed converter is fed back to the common DC source.

Although, motor emulator are existing for over two decades, there has been little to no research focus on simplifying the whole system by optimizing power converter topology used as an emulator. The converter topology used in [9] makes use of 17-level Double Star Chopper Cell (DSCC). The multilevel converter have their own advantages, however, the number of power semiconductor switches increase as the level increases resulting in increased switching losses. Therefore, as an attempt to simplify the whole ME architecture, including converter topology, this paper proposes a virtually isolated bidirectional three-phase AC-DC converter based on synchronous buck-boost operation. This paper follows the extended version of previous paper by authors [8] with slightly upgraded converter topology in terms of LCL filter replacing LC filter.

The organization of this paper is as follows. The conceptual introduction to existing ME system and common DC bus ME system are presented in Section–I along with research contribution of this paper. Section–II describes the operation of proposed bidirectional AC-DC converter along with voltage gain derivation in motoring as well as braking mode. The design of proposed converter is also presented in Section–III. The control scheme for common-DC-bus-configured ME system for emulating a PMSM motor are briefly discussed in Section–IV. Detailed experimental test results are presented

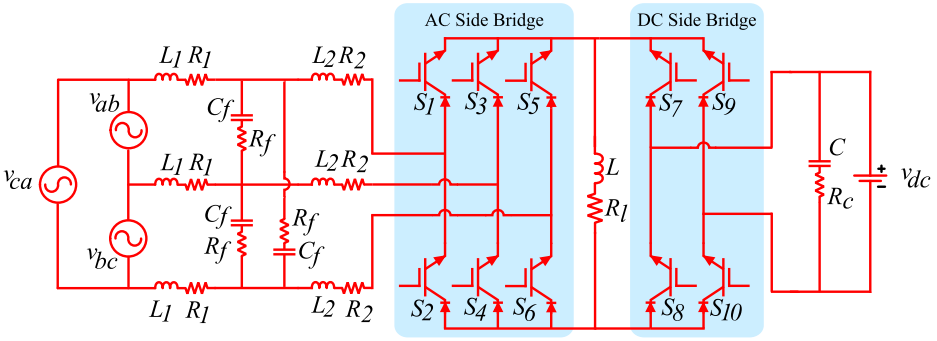

FIGURE 3. Proposed bi-directional buck-boost 3-ϕ AC-DC converter.

in Section–V for PMSM motor under study. Finally, proposed research work is concluded in Section–VI.

II. PROPOSED AC-DC CONVERTER

Numerous researchers have proposed 3-ϕ AC-DC converter topologies with buck, boost, buck-boost mode of operation [10]–[19]. A detailed review of three-phase AC-DC converter is presented by in [20]. A 3-ϕ step-down bi-directional AC-DC converter topology was proposed in [11]. A similar approach can be considered for 3-ϕ bi-directional AC-DC buck-boost converter. However, this would require twelve power semiconductor switches. A single-switch three-phase AC-DC converter topology was proposed in [12] and an upgraded topology was proposed in [13]. Another single switch buck-boost three-phase AC-DC converter topology was proposed in [14]. The three-phase diode bridge-rectifier, used in these topologies would block reverse power flow in braking mode. Thus, AC-DC converter with diode bridge rectifier, makes them unsuitable for the ME system. A three-phase single-stage AC-DC PWM full bridge converter was proposed in [15]. Although single-stage AC-DC conversion is possible, only the buck operation provided by this topology is not desired for ME application. Another interesting converter topology providing low current THD (*Total Harmonic Distortion*) was proposed in [16] consisting of buck-boost inductor in each leg of converter bridge. An isolated bi-directional AC-DC converter topology comprising of eighteen power semiconductor switches was proposed in [17], [18]. However, isolated converter topology is unsuitable for ME, as for low speed emulation, the isolation transformer coil magnetization is insufficient to generate secondary voltage, resulting in poor emulation performance. These factors associated with aforementioned converter topologies, highly demand a reduced switch, bi-directional, non-isolated AC-DC converter topology. In addition, single-stage reverse power control is also desired. Hence, for common DC bus ME application, with little modification in the 3-ϕ AC-DC converter topology presented in [19], a bi-directional buck-boost AC-DC converter topology was presented in [8]. The proposed converter topology has been improved from the one presented in [8] by authors. The *LC* filter in the converter topology presented in [8] has been replaced with *LCL* filter to reduce the stress on converter switches. Furthermore, the operating principle has also been modified to achieve desired buck-boost operation.

The proposed converter topology is presented in Fig. 3. For simple understanding of proposed converter operation, detailed schematic of common DC bus ME system along with proposed converter, control strategy and PMSM model are not shown here. The proposed converter in Fig. 3 replaces 'Bidirectional AC-DC Converter' block in Fig. 2. Referring to Fig. 3, three-phase unfiltered voltages, v_{ab}, v_{bc} and v_{ca} from DUT are applied as input to the proposed converter. On the output side, there is common DC bus, v_{dc}, which connects both ME output and DUT input. It is to be noted that, throughout this paper, v_{dc} represents common DC bus voltage. The output voltage of proposed converter is measured across DC Link capacitor C. Inductor L is buck-boost inductor, capacitor C is DC link capacitor.

The operation of proposed converter topology is further explained for forward motoring and forward braking mode of operation of AC machine. The operation of during reverse motoring and reverse braking is same as that of forward motoring and forward braking except the fact that, two of the three-phases are swapped. The operation of proposed converter is discussed based on SVPWM (space vector pulse width modulation) technique. It is well known phenomenon that, a SVPWM cycle comprises of two active vectors and one zero (null) vector. This phenomenon is used to achieve virtual isolation between the three-phase AC and DC sides of the proposed converter. During the active states, DC side full bridge of the proposed converter is virtually isolated as it is kept OFF for the entire active state duration. Whereas, during zero state, the energy stored in buck-boost inductor is dissipated into common DC bus through DC side full bridge. While in zero state, either all upper or lower switches from AC side three-phase bridge are ON, resulting in virtual isolation from DC side full bridge. Here, the duration of active vectors are denoted as T_1 and T_2, whereas that of zero vector is denoted as T_0. The AC side converter switches S_1 to S_6 forms a two-level PWM converter converting 3-ϕ input AC voltage from DUT to DC which appears across the buck-boost inductor L. At any instant the voltage appearing across inductor L is $(\sqrt{3} \cdot v_i)$, where v_i is input phase voltage.

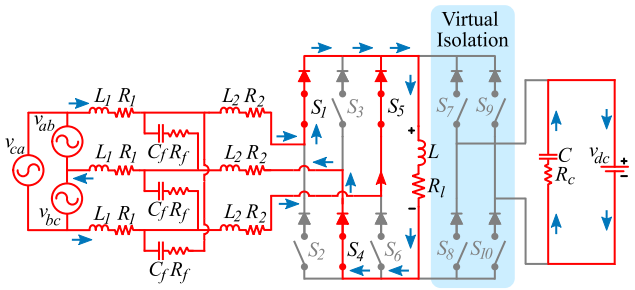

FIGURE 4. Forward motoring operation during active switching state - 101.

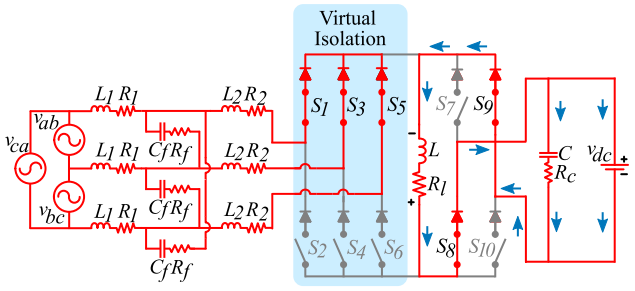

FIGURE 5. Forward motoring operation during zero switching state - 111.

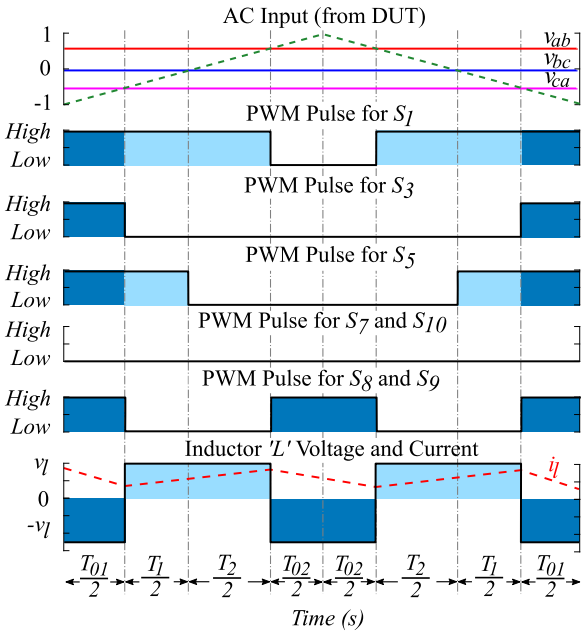

FIGURE 6. SVPWM switching pattern for forward motoring. [– Zero Vector Duration – Active Vector Duration.]

A. OPERATION: FORWARD MOTORING (QUADRANT-I)

In *forward motoring* operation, switch S_7 and S_{10} are kept *OFF* for the entire duration of *forward motoring* mode. In this mode of operation, energy is stored in buck-boost inductor L during active state. The current flow path for active state 101 is shown in Fig. 4.

During active state as shown in Fig. 4, based on the SVPWM control algorithm, the switches on AC side bridge turn *ON* and *OFF*, storing energy of the magnitude of V_l in inductor L.

$$V_l = L \times \frac{\delta I_l}{\delta t} \tag{1}$$

where, I_l is current through inductor L. The rise in inductor current I_l during both the active states is given by –

$$\Delta I_l(+) = \frac{(\sqrt{3} \cdot v_i - I_l \cdot R_l)}{L} \times T_{ON} \tag{2}$$

where, $T_{ON} = T_1 + T_2$, sum of two active vectors duration as shown in Fig. 4. For simplicity, the negligible voltage drop across switches is not considered here. The highlighted box in Fig. 4 shows the virtual isolation in proposed topology during active SVPWM (Space Vector PWM) states which isolates the DC link capacitor from buck-boost inductor. The SVPWM switching pattern for forward motoring operation is shown in Fig. 6.

During zero-state, as shown in Fig. 5, the polarity of inductor L reverses and the stored energy in L, dissipates through $L(+) \rightarrow S_8 \rightarrow v_{dc} \rightarrow S_9 \rightarrow L(-)$, performing forward motoring operation. During forward motoring, DC bus act as '*sink*', as the forward current flows into the DC bus V_{dc}.

The fall in inductor current I_l during zero switching state is given by –

$$\Delta I_l(-) = \frac{(V_c - I_l \cdot R_l)}{L} \times T_{OFF} \tag{3}$$

where, $T_{OFF} = T_0 = T_{01} + T_{02}$, zero switching state duration.

For steady-state operation, the rise in inductor current $\Delta I_l(+)$ and fall in inductor current $\Delta I_l(-)$ should be equal. Otherwise the cumulative increase or decrease in inductor current over a number of switching cycles would result in unstable condition. Therefore, by equating (2) and (3), output voltage for forward motoring operation i.e. capacitor voltage V_c can be estimated as –

$$V_c = \sqrt{3} \cdot v_i \times \frac{T_{ON}}{T_{OFF}} \tag{4}$$

Here, the impedance R_l of inductor L is small enough to be neglected. Therefore, second term $I_l \cdot R_l$ in (2) and (3) are neglected in (4). Furthermore, substituting $D = T_{ON}/T_s$ and $(1-D) = T_{OFF}/T_s$, where $T_s = T_{ON} + T_{OFF}$, the steady-state output voltage equation (4) can be rewritten as –

$$V_c = \sqrt{3} \frac{D}{(1-D)} v_i \tag{5}$$

B. OPERATION: FORWARD BRAKING (Quadrant-II)

In *forward braking* operation, the torque direction reverses while speed direction remains same as that of *forward motoring*. However, during this mode of operation the DUT output voltage and current are 180° out of phase. This results in reverse current flow from DC side of the converter to AC side. During this mode of operation, switches S_8 and S_9 are kept continuously *OFF* while switches S_7 and S_{10}, are switched *ON* and *OFF* simultaneously during zero switching

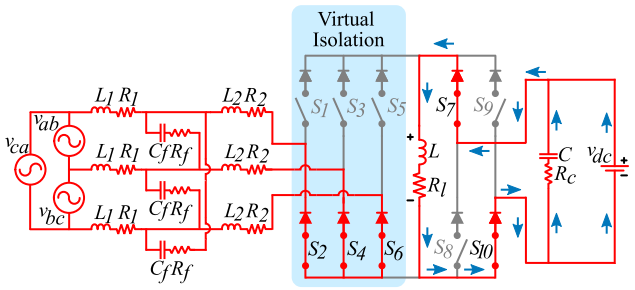

FIGURE 7. Forward braking operation during zero switching state - 000.

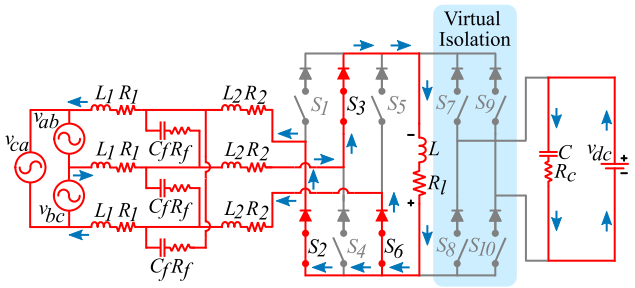

FIGURE 8. Forward braking operation during active switching state - 010.

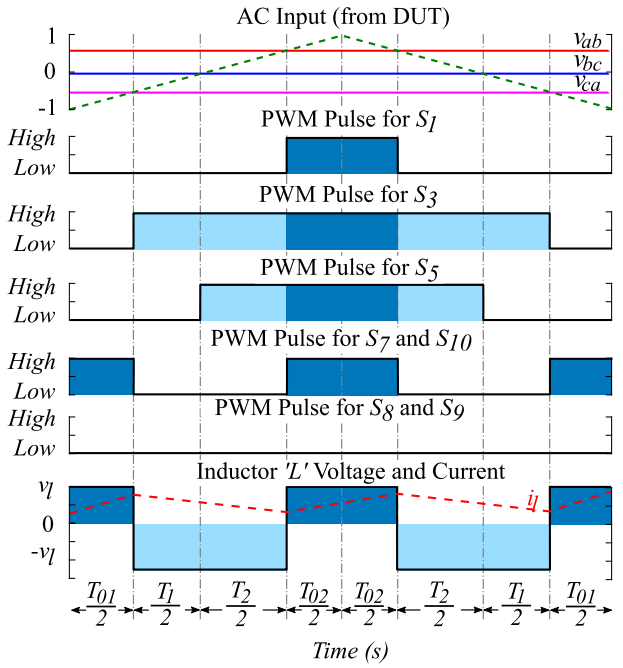

FIGURE 9. PWM switching pattern for forward braking. [– Zero Vector Duration – Active Vector Duration].

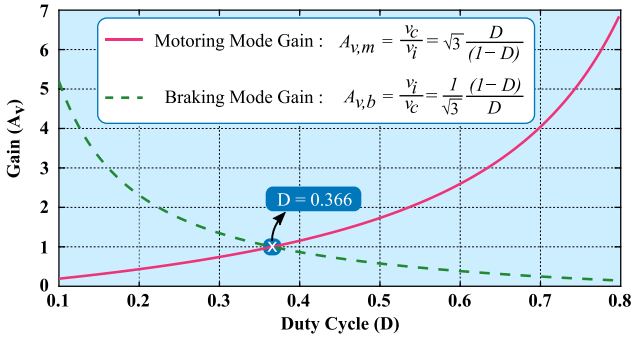

FIGURE 10. Voltage gain curve for motoring and braking mode of operation.

state. This causes the current to flow from DC side source $v_c(+) \rightarrow S_7 \rightarrow L \rightarrow S_{10} \rightarrow V_c(-)$, completing the closed path as shown in Fig. 7. As the current flows through inductor L, an energy of the magnitude of v_l is stored in it. The rise in current $I_l(+)$ during this period is given by (3) i.e.–

$$\Delta I_l(+) = \frac{(V_c - I_l \cdot R_l)}{L} \times T_{OFF} \tag{6}$$

This stored energy in inductor L, then dissipates stored energy through AC side converter switches. For the duration of forward breaking, according to control strategy implemented, the AC sided bridge switching allows reverse flow of current back to DUT as shown in Fig. 8. At the same time, according to the control algorithm for DUT, ME terminal voltage is maintained positive with respect to the reference voltage. The fall in inductor current I_l during both the active states is given by –

$$\Delta I_l(-) = \frac{(\sqrt{3} \cdot v_i - I_l \cdot R_l)}{L} \times T_{ON} \tag{7}$$

Solving (6) and (7) for output voltage in forward braking operation, i.e. v_{phase} in this case, gives –

$$V_i = \frac{1 - D}{\sqrt{3} \cdot D} v_c \tag{8}$$

The switching patterns during forward breaking operation is shown in Fig. 9. As opposed to forward-motoring, in forward-braking mode, the energy is stored in inductor L during zero switching state. Whereas, it is dissipated during active switching state.

The voltage gain expression for motoring operation can be derived from (5) as–

$$\therefore A_{v,m} = \frac{v_c}{v_i} = \sqrt{3}\frac{D}{(1 - D)} \tag{9}$$

The gain expression derived in (9) is valid for motoring operation during first and third quadrant. Similarly, voltage gain ($A_{v,b}$) for braking operation can be derived from (8) as –

$$A_{v,b} = \frac{v_i}{v_c} = \frac{1}{\sqrt{3}}\frac{(1 - D)}{D} \tag{10}$$

The voltage gain curves, for expressions derived in (9) and (10), for motoring as well as braking modes of operation respectively, are shown in Fig. 10. The gain curves are plotted for duty cycle D ranging from 0.1 to 0.8. This is because of the theoretically infinite gain possible above $D = 0.8$, using (9) and below $D = 0.1$, using (10). As shown in Fig. 10, the buck

TABLE 1. Summary of Proposed Converter Switching.

Torque Reference	Speed Reference	Operating Mode	Quadrant	Input Phase Difference			Comparator Operator	Energy Storage in 'L'		Energy Dissipation from 'L'		DC Bus *act as*
				v_{ab}	v_{bc}	v_{ca}		*During*	*Through*	*During*	*Through*	
Positive	Positive	Forward Motoring	I	0°	−120°	−240	$v_{tri} \leq v_i$	Active Vector	S_1 to S_6	Zero Vector	S_7 and S_{10}	'Sink'
Negative	Positive	Forward Braking	II	0°	−120°	−240	$v_{tri} \geq v_i$	Zero Vector	S_7 and S_{10}	Active Vector	S_1 to S_6	'Source'
Negative	Negative	Reverse Motoring	III	0°	−240°	−120	$v_{tri} \leq v_i$	Active Vector	S_1 to S_6	Zero Vector	S_7 and S_{10}	'Sink'
Positive	Negative	Reverse Braking	IV	0°	−240°	−120	$v_{tri} \geq v_i$	Zero Vector	S_7 and S_{10}	Active Vector	S_1 to S_6	'Source'

v_{tri}: triangular carrier signal; v_i: modulating input signal (where, i = *phase – a, b or c*)

to boost and vice-versa crossover occurs at $D = 0.37$ duty cycle.

The four quadrant control and switching of proposed converter is summarized in Table - 1.

III. DESIGN AND PROTOTYPE OF PROPOSED CONVERTER

A. CONVERTER DESIGN

Design is the very important aspect for achieving desired output, for any power converter. The proposed bidirectional converter consist of an energy storage element between AC and DC sides switching bridge serving as buck-boost inductor and a LCL filter between DUT and AC side input terminals of converter. In addition to these components, a capacitor on DC side serve as DC link element.

The LCL filter is designed following the procedure provided in [21] and [22] and therefore the design formulas are not repeated here. The proposed bidirectional converter is designed for a 10 kW ME system using design expressions presented below and the parameters are listed in Table - 2.

TABLE 2. Proposed Converter Design Specifications.

Parameter	Symbol	Value	
DC Bus Voltage	v_{dc}	500.00	V
Input Filter Inductor	L_1	1.9	mH
Filter Capacitor	C_f	10.22	μF
Output Filter Inductor	L_2	37.18	μH
Energy Storage Inductor	L	1.7	mH
DC Link Capacitor	C	3500.00	μF
Switching Frequency	F_s	20.00	kHz
Output Power	P_o	10.00	kW

1) ENERGY STORAGE INDUCTOR (L)

For Buck mode, neglecting ESR and assuming 20% allowable current ripple, the energy storage inductor L can be estimated as –

$$L > \frac{v_{dc}}{x \times (i_{l,max} - i_{l,min}) \times F_s} \tag{11}$$

where,

$i_{l,max}$ = maximum current through inductor L,

$i_{l,min}$ = minimum current through inductor L,

F_s = switching frequency, and

x = estimated coefficient for amount of ripple current allowed (typically between 0.2 to 0.4).

Similarly, for boost mode –

$$L > \frac{\sqrt{3} \cdot v_i}{x \times (i_{l,max} - i_{l,min}) \times F_s} \tag{12}$$

where, v_i is line to line input voltage.

For the design of converter, the inductor with higher inductance among (11) and (12) should be selected.

2) DC LINK CAPACITOR (C)

The size of DC link capacitor can be estimated using the expression for energy stored in the capacitor. The energy stored in capacitor is given by the relation $0.5\,Cv^2$. Using this relation the DC capacitor value can be estimated by –

$$C = \frac{2 \times P}{(v_{c,max} - v_{c,min})^2 \times F_r} \tag{13}$$

where, P is power capacity of converter and F_r is emulator converter rectification frequency

B. HARDWARE SETUP

The proposed ME converter for design parameters listed in Table - 2, has been developed for experimental testing. The developed setup is as shown in Fig. 11. As, drive under test (DUT), an off-the-shelf Semikron inverter module (SEMITEACH B6U+E1CIF+B6CI) is used, which is controlled by Texas Instruments DSP TMS320F28337D. High precision LEM voltage and current sensors are used for voltage and current sensing. The voltage sensor LV-20P has the capability of sensing $0 - 500$ V AC or DC voltage with sensed output up to ± 15 V. Similarly, current sensor LTS-25 from LEM used in developed setup can sense up to 25 A AC or DC current with proportional output voltage varying from 0 V to 5 V DC. The proposed converter is developed using 600 V/85 A Reverse-Blocking IGBT (RB-IGBT) FGW85N60RB from Fuji Electric. Two RB-IGBT's are used in series at each switch place (S_1 to S_{10}) in proposed converter to make up for the desired voltage rating of 1200 V of each switch. The controller used for proposed converter is

TABLE 3. List of Components and Laboratory Equipment used for Experimental Setup.

	Part # (Manufacturer)	Ratings
Device Under Test (DUT)	SEMITEACH (Semikron)	750 V DC In 400 V AC Out
DUT Microcontroller	F28069M (Texas Instru.)	90 MHz
Voltage Sensor	LV–20P (LEM)	0-500 V AC/DC In ± 15 V AC Out
Current Sensor	LTS–25 (LEM)	25 A AC/DC In 0–5 V DC Out
Emulator Converter Power Switch	FGW85N60RB (Fuji Electric)	600 V / 85 A
Emulator Microcontroller	TMS320F28335 (Texas Instru.)	150 MHz
DC Power Supply	RP7951 (KEYSIGHT)	0-500 V DC / 10 A / 5 kW

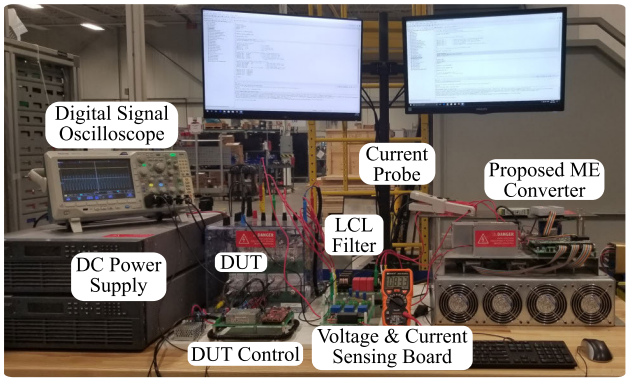

FIGURE 11. Hardware setup of proposed ME system.

TMS320F28335 from Texas Instruments Inc. Two DC power supplies of 500 V, 5 kW capacity are used in parallel to supply 10 kW power to common DC bus. The experimental setup details are listed in Table - 3.

IV. CONTROL OF PROPOSED ME SYSTEM

The DUT used for experimentation is a standard two-level AC-DC converter, controlled using vector control method with switching frequency of 20 kHz. However, ME system is expected to be independent of DUT converter topology and its control algorithm has to exclusively emulate electric motor characteristics. In addition, the DUT drive topology and its control can vary from customer-to-customer as per system requirements. Therefore, detailed explanation of DUT control drive is out of the scope of this paper.

Proposed ME converter operation, voltage gain and state-space model have already been discussed in detail in previous sections. Since, the focus of this paper is on proposed converter topology for ME application, the control strategy used to control ME converter is briefly discussed in this section.

A. PMSM MOTOR MATHEMATICAL MODEL

The PMSM motor mathematical model from [23], is implemented in digital controller. The direct and quadrature axis current are estimated as –

$$\frac{d}{dt}i^r_{ds} = \frac{1}{L_d}v^r_{ds} - \frac{R_s}{L_d}i^r_{ds} + \frac{L_q}{L_d}\omega_r i^r_{qs} \tag{14}$$

$$\frac{d}{dt}i^r_{qs} = \frac{1}{L_q}v^r_{qs} - \frac{\lambda_m}{L_q}\omega_r - \frac{R_s}{L_q}i^r_{qs} - \frac{L_d}{L_q}\omega_r i^r_{ds} \tag{15}$$

For a PMSM motor, the electromagnetic torque T_e is –

$$T_e = \left(\frac{3}{2}\right)\left(\frac{p}{2}\right)\left(\lambda_m i_{qs} + (L_d - L_q)i_{qs}i_{ds}\right) \tag{16}$$

where, 'p' is the number of poles and λ_m is magnetic flux linkage. L_q and L_d are quadrature and direct axis inductances as well as i_{qs} and i_{ds} are quadrature and direct axis currents.

Since, the i_{ds} for PMSM motor is zero, eq. (16) becomes,

$$T_e = \frac{3 \cdot P \cdot \lambda_m}{2} \cdot i_{qs} \tag{17}$$

where, 'P' is number of pole pairs. This T_e, estimated by motor model is used to estimate reference current i^*_q, whereas i^*_d for PMSM motor is zero.

$$\therefore i^*_{qs} = \frac{2}{3 \cdot P \cdot \lambda_m} \cdot T_e \tag{18}$$

and,

$$i^*_{ds} = 0 \tag{19}$$

B. PROPOSED CONVERTER MATHEMATICAL MODEL

The block diagram of proposed converter's mathematical model in dq coordinate system is shown in Fig. 12. The corresponding voltage and current quantities in dq coordinates at each of the node of proposed topology are represented by their respective suffix letter d or q. The current through energy storage inductor L, is represented by i_l.

The output of the proposed converter is dc current i_{dc2} flowing into the DC bus during motoring mode of operation as shown in Fig. 12(a). The direction of i_{dc2} reverses during braking mode of operation as shown in Fig. 12(b). From the operating principle of proposed converter, it is evident that during motoring mode, the energy stored in inductor L, dissipates into DC bus as i_{dc2}, *i.e.* $i_l = i_{dc2}$. Similarly, during braking mode, energy is stored into inductor L. The current i_l

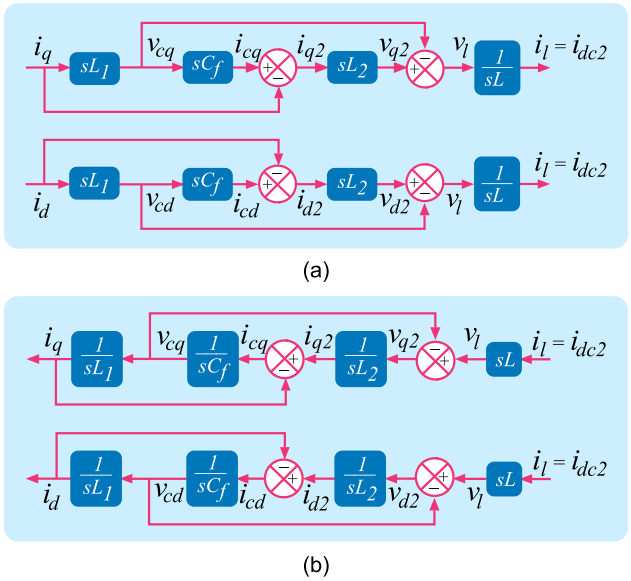

FIGURE 12. Mathematical model of proposed converter topology in *dq* coordinate system. (a) Motoring mode (b) Braking Mode.

profile, carries information of both rising and falling edge of current i_{dc2}. Whereas, the DC side converter bridge is virtually isolated during zero switching state allowing current i_{dc2} being discontinuous. Therefore, current i_l can be considered as the output control variable to represent converter transfer function in motoring mode.

To efficiently and accurately emulate the behavior of AC machine, the phase, frequency and magnitude of the AC current must be taken into account. Inductor current i_l, being DC quantity, does not account for phase, frequency and magnitude. Also, the DUT output current

C. CONTROL STRATEGY

Similarly, the three-phase current output from DUT is transformed into two-phase quantities using park's transformation to estimate real direct and quadrature axis currents,i_d and i_q, supplied by DUT to emulator.

$$\begin{bmatrix} i_{qs} \\ i_{ds} \end{bmatrix} = \frac{2}{3} \begin{bmatrix} -sin(\omega t) & -sin(\omega t - \frac{2\pi}{3}) & -sin(\omega t + \frac{2\pi}{3}) \\ cos(\omega t) & cos(\omega t - \frac{2\pi}{3}) & cos(\omega t + \frac{2\pi}{3}) \end{bmatrix} \begin{bmatrix} i_a \\ i_b \\ i_c \end{bmatrix}$$

The calculated real i_ds and i_qs are then compared with their corresponding reference values i.e. i_d^* and i_q^*. The errors of two are then controlled using individual PI controllers which produces v_{qs}^* and v_{ds}^* as output signals respectively.

$$v_{qs}^* = \left(K_p + \frac{K_i}{s}\right) \cdot (i_{qs}^* - i_{qs}) \tag{20}$$

and,

$$v_{ds}^* = \left(K_p + \frac{K_i}{s}\right) \cdot (i_{ds}^* - i_{ds}) \tag{21}$$

The two-phase direct and quadrature axis voltage quantities, v_{qs}^* and v_{ds}^*, are then transformed to *a-b-c* quantities to generate sinusoidal template, v_{abc} for carrier based SVPWM generation. The voltage template v_{abc}, is proportional to the amount of voltage required to be applied across inductor L, to allow the matching current to be drawn from DUT with that of reference current.

The operation of the proposed ME system is divided into four quadrants. The reference torque and speed signals are used to decide the quadrant of operation according to Table - 1. As per quadrant of operation, comparator operator is selected to compare v_{abc} with v_{tri} for SVPWM generation. The generated PWM pulses are further used, to drive proposed ME converter.

It is to be noted that, carrier based SVPWM technique calculates switching (ON and OFF) time duration for AC side converter switches. However, DC side converter switches are activated during zero switching state and according to quadrant of operation as summarized in Table - 1.

TABLE 4. Motor Parameters.

Motor Parameter	Nomenclature	Value
Rated Power	P_m	7.5 kW
Rated Speed	ω_r	1800 rpm
Rated Torque	T_r	14 $N \cdot m$
Rated Current	I_r	14 A
Number of Poles	P	6
Stator Resistance	R_s	0.348 Ω
Stator d-axis Inductance	L_d	3 mH
Stator q-axis Inductance	L_q	14.9 mH
Magnetic Flux	λ	0.22 Vs/rad

TABLE 5. Speed and Torque Input Test Commands for Experimental Testing.

Operating Mode	Quadrant	Load Torque		Rotor Speed	
		(T_L^*)	Step-Time	($\omega_m{}^*$)	Step-Time
Forward Motoring	I	10 Nm	0.0 s	500 RPM	0.0 s
Forward Braking	II	-10 Nm	3.0 s	900 RPM	4.0 s
Reverse Motoring	III	-10 Nm	7.0 s	-500 RPM	8.0 s
Reverse Braking	IV	10 Nm	18.0 s	-900 RPM	15.0 s

V. EXPERIMENTAL TEST RESULTS ANALYSIS

The proposed converter topology is experimentally developed and tested for the motor parameters listed in Table - 2 and 4 and test conditions listed in Table - 5 respectively.

Figure 13 to 17 shows experimental results for all test commands listed in Table - 5. The phase-A current waveform for current drawn from DUT is displayed on channel CH-1. The signals on channel CH-3 and CH-4 on Fig. 13 to 17 are rotor speed and electromagnetic torque estimated by motor model respectively. These speed and torque signals are displayed on oscilloscope through DAC pin of DSP controller.

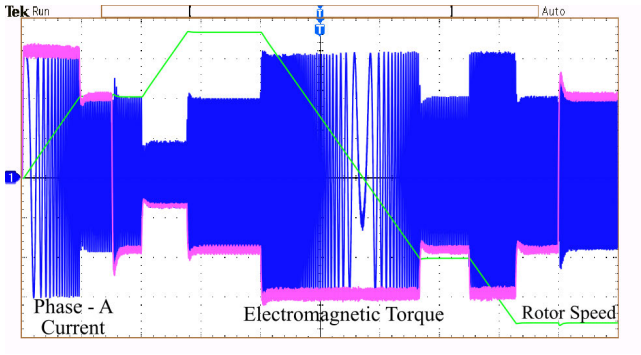

FIGURE 13. Experimental results for PMSM motor. CH-1: 5A/div CH-3: 5V/div(1V/50 RPM) CH-4: 5V/div(1V/Nm) X-axis : 2.0 s/div.

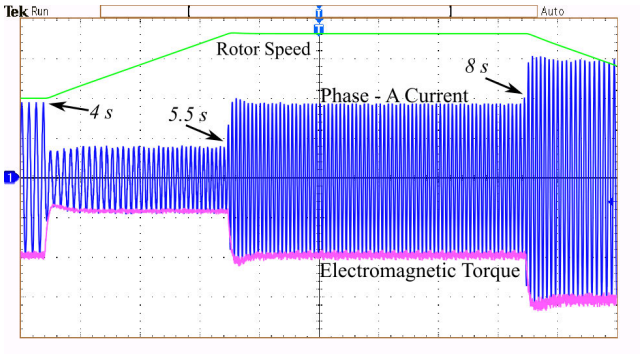

FIGURE 15. Experimental results (Zoomed view of Fig. 13 from 4s to 8s). CH-1: 5A/div CH-3: 5V/div(1V/50 RPM) CH-4: 5V/div(1V/Nm) X-axis : 0.5 s/div.

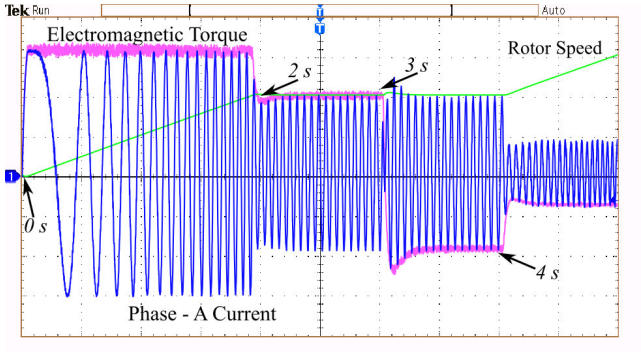

FIGURE 14. Experimental results (Zoomed view of Fig. 13 from 0s to 5s). CH-1: 5A/div CH-3: 5V/div(1V/50 RPM) CH-4: 5V/div(1V/Nm) X-axis : 0.5 s/div.

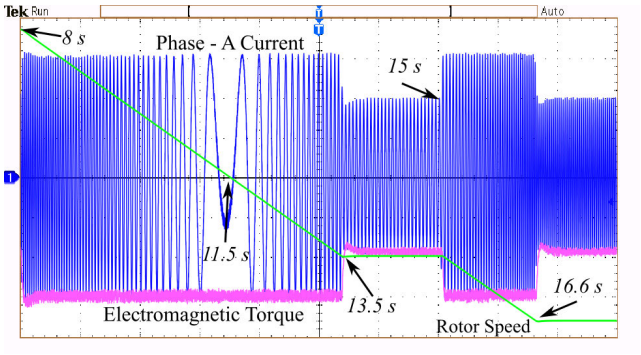

FIGURE 16. Experimental results (Zoomed view of Fig. 13 from 8s to 18s). CH-1: 5A/div CH-3: 5V/div(1V/50 RPM) CH-4: 5V/div(1V/Nm) X-axis : 0.5 s/div.

The results for all four quadrants are shown in Fig. 13 for various torque and speed test commands. As shown in Fig. 14, at time $t = 0$ *s*, both speed and torque commands are set to 500 *RPM* and 10 *Nm* respectively. With these test commands, the emulator is expected to emulate first quadrant (forward motoring) of operation of PMSM motor under study. Until 2 *s*, when motor attains desired 500 *RPM* speed, the emulator draws high current to emulate high starting torque as can be seen in Fig. 14. As soon as the emulated speed reaches to desired speed reference, emulator starts drawing nominal current and electromagnetic torque drops down to its reference value i.e. 10 *Nm*. The torque remains constant to 10 *Nm* until the next test command, which appears at 3 *s*. For initial three seconds, the ME system emulates forward motoring operation.

At 3 *s*, the torque command changes to -10 *Nm* to force emulation of forward braking operation. It is visible in Fig. 14 that, as soon as the torque command changes the, the emulated torque drops to -10 *Nm* and phase-A current reverses. A minor spike in current as well as speed waveform can be noticed in Fig. 14. However, emulator still draws, the 10 *A* peak current from DUT. At 4 *s*, the speed reference is changed to 900 *RPM* and to operate in constant torque region, the electromagnetic torque increases from -10 *Nm* to -4 *Nm*.

At 5.5 *s*, the emulator speed attains the desired reference of 900 *RPM* as shown in Fig. 15. The electromagnetic torque returns to the -10 *Nm* reference mark and remains steady until next test command appears at 8 *s*. As the speed reference is dropped to -500 *RPM* at 8 *s*, the braking current increases to approximately 15 *A* peak. The emulator, draws high braking current until rotor speed is dropped to zero at approx. 11.5 *s*. At this instance, the forward braking operation ends.

At 11.5 *s*, speed as well as phase reversal occurs as shown in Fig. 16. The emulated rotor speed further drops linearly in negative direction (reverse motoring) until desired speed is attained at 13.5 *s*. The electromagnetic torque returns to its reference value of -10 *Nm* and remains constant until next test command appears at 15 *s*. At 15 *S*, the reference speed is further increased in reverse direction to -900 *RPM*, as shown in Fig. 16. The DUT supplies, the high current demand during speed increment until speed is reached to -900 *RPM* at 16.6 *s*. The reverse motoring operation continues till 18.0 *s* when next test command appears.

As shown in Fig. 17, at 18.0 *s*, the torque reference is changed from -10 *Nm* to 10 *Nm*, to force reverse braking operation. This sudden braking causes minor spike in current signal, as can be noticed in Fig. 17.

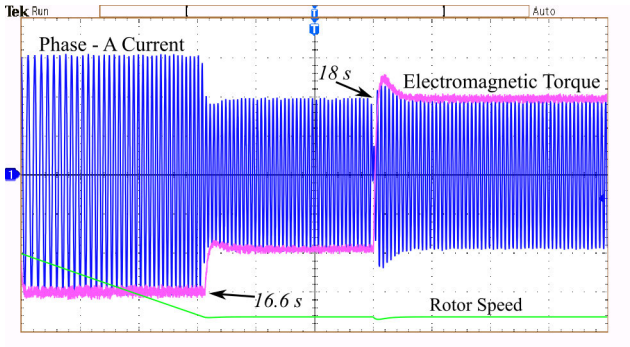

FIGURE 17. Experimental results (Zoomed view of Fig. 13 from 15s to 20s). CH-1: 5A/div CH-3: 5V/div(1V/50 RPM) CH-4: 5V/div(1V/Nm) X-axis : 0.5 s/div.

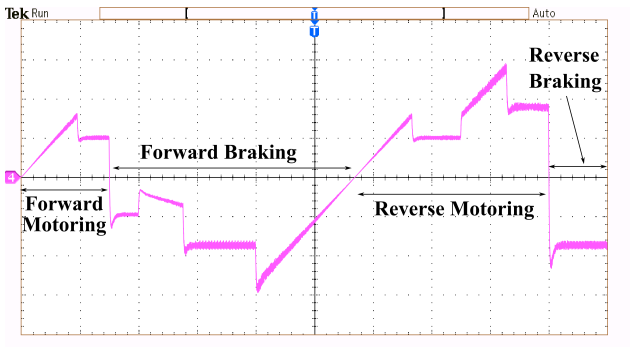

FIGURE 18. DC bus current at the output of proposed emulator converter. CH-4: 5A/div X-axis : 2.0 s/div.

Figure 18, shows the DC bus current at the output of proposed emulator converter. It can be seen in the Fig. 18 that, during forward as well as reverse motoring operation, the emulator converter output current is pumped back into DC bus. Similarly, during forward and reverse braking mode of operation, the DC side of proposed converter act as input and draws power from DC bus. The negative current during both braking regions verifies the bidirectional operation of proposed converter.

VI. CONCLUSION

A simplified virtually isolated, bidirectional, three-phase AC-DC converter for ME system is proposed in this paper. The proposed bi-directional converter inspired from classical buck-boost operation, requires just ten unidirectional IGBT switches. The unidirectional IGBT swtiches prevents any circulating current in the system. The proposed converter also takes out the regenerative converter stage in classical ME system. Also, the proposed common DC-bus-configured ME system requires a single stage control unlike independent control in existing ME system. The proposed converter provides four-quadrant operation and emulation of motor under study. From the experimental results, it is concluded that, with the presented control scheme in section - V, the proposed ME converter can be made to draw the same current as a real machine would have drawn, had it been driven by the same DUT. The PMSM motor model is used to estimate the reference current used for controlling the proposed converter. This provides re-configuration ability to ME system. Since, the DC output current of proposed converter is fed back to DC bus, the overall input power source requirement is reduced.

Overall, by analyzing experimental results, it is verified that, proposed virtually isolated, bidirectional AC-DC converter topology is a feasible alternative for conventional ME system with AC-DC-AC converter, providing simple common control.

REFERENCES

[1] R. S. Kaarthik, K. S. Amitkumar, and P. Pillay, "Emulation of a permanent-magnet synchronous generator in real-time using power hardware-in-the-loop," *IEEE Trans. Transport. Electrific.*, vol. 4, no. 2, pp. 474–482, Jun. 2018.

[2] K. S. Amitkumar, R. S. Kaarthik, and P. Pillay, "A versatile power-hardware-in-the-loop-based emulator for rapid testing of transportation electric drives," *IEEE Trans. Transport. Electrific.*, vol. 4, no. 4, pp. 901–911, Dec. 2018.

[3] M. Oettmeier, R. Bartelt, C. Heising, V. Staudt, A. Steimel, S. Tietmeyer, B. Bock, and C. Doerlemann, "Machine emulator: Power-electronics based test equipment for testing high-power drive converters," in *Proc. 12th Int. Conf. Optim. Electr. Electron. Equip.*, May 2010, pp. 582–588.

[4] Y. S. Rao and M. C. Chandorkar, "Real-time electrical load emulator using optimal feedback control technique," *IEEE Trans. Ind. Electron.*, vol. 57, no. 4, pp. 1217–1225, Apr. 2010.

[5] O. Vodyakho, M. Steurer, C. S. Edrington, and F. Fleming, "An induction machine emulator for high-power applications utilizing advanced simulation tools with graphical user interfaces," *IEEE Trans. Energy Convers.*, vol. 27, no. 1, pp. 160–172, Mar. 2012.

[6] D. J. Atkinson, A. G. Jack, and H. J. Slater, "The virtual machine [power electronic conversion equipment testing]," in *Proc. IEE Colloq. Vector Control*, Feb. 1998, pp. 7-1–7-6.

[7] J. W. Kolar, T. Friedli, J. Rodriguez, and P. W. Wheeler, "Review of three-phase PWM AC–AC converter topologies," *IEEE Trans. Ind. Electron.*, vol. 58, no. 11, pp. 4988–5006, Nov. 2011.

[8] A. H. Kadam, R. Menon, and S. S. Williamson, "A novel bidirectional three-phase AC–DC/DC-AC converter for PMSM virtual machine system with common DC bus," in *Proc. IEEE Appl. Power Electron. Conf. Expo. (APEC)*, San Antonio, TX, USA, Mar. 2018, pp. 1944–1951.

[9] K. Saito and H. Akagi, "A real-time real-power emulator of a medium-voltage high-speed induction motor loaded with a centrifugal compressor," *IEEE Trans. Ind. Appl.*, vol. 55, no. 5, pp. 4821–4833, Sep. 2019.

[10] I. Abdelsalam, G. P. Adam, D. Holliday, and B. W. Williams, "Single-stage AC–DC buck-boost converter for medium-voltage high-power applications," *IET Renew. Power Gener.*, vol. 10, no. 2, pp. 184–193, 2016.

[11] T. C. Green, M. H. Taha, N. A. Rahim, and B. W. Williams, "Three-phase step-down reversible AC–DC power converter," *IEEE Trans. Power Electron.*, vol. 12, no. 2, pp. 319–324, Mar. 1997.

[12] E. H. Ismail and R. Erickson, "Single-switch 3-ϕ PWM low harmonic rectifiers," *IEEE Trans. Power Electron.*, vol. 11, no. 2, pp. 338–346, Mar. 1996.

[13] D. S. Wijeratne and G. Moschopoulos, "A novel three-phase buck–boost AC–DC converter," *IEEE Trans. Power Electron.*, vol. 29, no. 3, pp. 1331–1343, Mar. 2014.

[14] I. Abdelsalam, G. P. Adam, D. Holliday, and B. W. Williams, "Three-phase AC–DC buck-boost converter with a reduced number of switches," *IET Renew. Power Gener.*, vol. 9, no. 5, pp. 494–502, 2015.

[15] D. S. Wijeratne and G. Moschopoulos, "A three-phase single-stage AC–DC PWM buck-type full-bridge converter: Analysis, design, and characteristics," *IEEE Trans. Ind. Electron.*, vol. 60, no. 10, pp. 4201–4214, Oct. 2013.

[16] L.-S. Yang, T.-J. Liang, and J.-F. Chen, "Analysis and design of a novel three-phase AC–DC buck-boost converter," *IEEE Trans. Power Electron.*, vol. 23, no. 2, pp. 707–714, Mar. 2008.

[17] L. Gu and K. Jin, "A three-phase isolated bidirectional AC/DC converter and its modified SVPWM algorithm," *IEEE Trans. Power Electron.*, vol. 30, no. 10, pp. 5458–5468, Oct. 2015.

[18] L. Gu and K. Jin, "A three-phase bidirectional AC/DC converter with Y-△ connected transformers," *IEEE Trans. Power Electron.*, vol. 31, no. 12, pp. 8115–8125, Dec. 2016.
[19] V. F. Pires and J. F. A. Silva, "Single-stage three-phase buck-boost type AC–DC converter with high power factor," *IEEE Trans. Power Electron.*, vol. 16, no. 6, pp. 784–793, Nov. 2001.
[20] B. Singh, B. N. Singh, A. Chandra, K. Al-Haddad, A. Pandey, and D. P. Kothari, "A review of three-phase improved power quality AC–DC converters," *IEEE Trans. Ind. Electron.*, vol. 51, no. 3, pp. 641–660, Jun. 2004.
[21] M. Liserre, F. Blaabjerg, and S. Hansen, "Design and control of an LCL-filter-based three-phase active rectifier," *IEEE Trans. Ind. Appl.*, vol. 41, no. 5, pp. 1281–1291, Sep. 2005.
[22] A. Reznik, M. G. Simões, A. Al-Durra, and S. M. Muyeen, "LCL filter design and performance analysis for grid-interconnected systems," *IEEE Trans. Ind. Appl.*, vol. 50, no. 2, pp. 1225–1232, Mar. 2014.
[23] A. H. Kadam, R. Menon, and S. S. Williamson, "Traction inverter performance testing using mathematical and real-time controller-in-the-loop permanent magnet synchronous motor emulator," in *Proc. 42nd Annu. Conf. IEEE Ind. Electron. Soc. (IECON)*, Oct. 2016, pp. 6651–6656.

ARVIND H. KADAM (Member, IEEE) received the B.Eng. degree in electronics and the M.Eng. degree in power electronics and drives from the University of Mumbai, Mumbai, India, in 2009 and 2013, respectively. He is currently pursuing the Ph.D. degree in power electronics and drives with the Department of Electrical, Computer and Software Engineering, Ontario Tech University, Oshawa, Canada. His research interests include the areas of power electronic converters and DSP applications in power electronics. He is a member of the Smart Transportation Electrification and Energy Research (STEER) Group, Ontario Tech University, headed by Dr. Sheldon Williamson.

SHELDON S. WILLIAMSON (Fellow, IEEE) received the B.E. degree (Hons.) in electrical engineering from the University of Mumbai, Mumbai, India, in 1999, and the M.S. and Ph.D. degrees (Hons.) in electrical engineering from the Illinois Institute of Technology, Chicago, IL, USA, in 2002 and 2006, respectively.

He is currently a Professor with the Department of Electrical, Computer and Software Engineering and the Director of Smart Transportation Electrification and Energy Research (STEER) Group, Faculty of Engineering and Applied Sciences, Ontario Tech University, Oshawa, ON, Canada. His current research interests include advanced power electronics, electric energy storage systems, and motor drives for transportation electrification. He holds the prestigious NSERC Canada Research Chair position in electric energy storage systems for transportation electrification.